Roughness-Adaptive 3D Watermarking Based on Masking Effect of Surface Roughness

Kwangtaek Kim, *Student Member, IEEE,* Mauro Barni, *Senior Member, IEEE,* and Hong Z. Tan, *Senior Member, IEEE*

Abstract—We present a general method to improve watermark robustness by exploiting the masking effect of surface roughness on watermark visibility. Our idea is to adapt watermark strength to local surface roughness based on the knowledge that human eyes are less sensitive to changes on a rougher surface patch than those on a smoother surface. In order to quantify human sensitivity to surface roughness of polygonal meshes, we conducted a rigorous psychovisual experiment to obtain human watermark detection thresholds as a function of surface roughness. The results were used for adaptively selecting watermark strength according to local surface roughness during the watermark embedding process. To test our general idea, we applied it to the modified versions of two popular 3D watermarking methods, one proposed by Benedens [1] and one by Cayre & Macq [2]. Experimental results showed that our approach improves watermark robustness as compared to the original algorithms. Further analyses indicated that the average watermark strength allowed by our roughness-adaptive method was larger than that by the original Benedens's and Cayre & Macq's methods while ensuring watermark imperceptibility. This was the main reason for the improved robustness observed in our experiments. We conclude that exploiting the masking property of human vision is a viable way to improve the robustness of 3D watermarks, and can potentially be applied to other 3D digital watermarking techniques.

Index Terms—Roughness-adaptive 3D watermarking, robustness, masking effect, polygonal mesh, surface roughness

I. INTRODUCTION

WITH advances of computer graphics technology, 3D digital contents have become increasingly popular in many applications such as video games, CAD (computer-aided design), VR (virtual reality), TV broadcasting, and medical imaging. Through the internet access, 3D digital contents are getting widely distributed or manipulated, often without copyright protection. For this reason, developing watermarking algorithms for 3D polygonal meshes has received more interests than before. Compared to 2D digital watermarking, however, 3D watermarking is more difficult due to the increased complexity associated with arbitrary shapes. 3D watermarks are more fragile due to the various ways that embedded watermarks can be destroyed by simply altering the meshes making up the 3D objects. Therefore, existing 2D watermarking techniques cannot be directly applied to

K. Kim and H.Z. Tan are with the Haptic Interface Research Laboratory, Purdue University, West Lafayette, IN 47907-2035.

Email: samuelkim@purdue.edu, hongtan@purdue.edu.

Mauro Barni is with the Department of Information Engineering, University of Siena, via Roma 56, 53100, Siena, Italy.

Email: barni@dii.unisi.it

3D models, thereby necessitating new approaches that are specifically designed for 3D objects.

The challenge is to design 3D digital watermarks that are *unobtrusive (transparent)*, *robust*, and *space efficient (capacity)*[3]. The *unobtrusive* requirement means that the embedded watermark should not interfere with the intended use of a model, which may imply imperceptibility. *Robustness* refers to the ability for the watermark to survive various intentional and unintentional attacks to the watermarked 3D model. This is a very challenging requirement as no algorithm has been shown to be perfectly robust. However, constant improvements are being made that result in more robust watermarking schemes as compared to previous methods. The last requirement is about having enough space for watermark embedding. To meet all three requirements at the same time is not trivial.

Of the three requirements, *unobtrusiveness* and *robustness* conflict with each other. From an *unobtrusiveness* perspective, watermark strength should be smaller in order to be imperceptible. From a *robustness* perspective, however, watermark strength should be larger so that the watermark can not be easily destroyed. It is a trade-off to satisfy both requirements at the same time.

In an effort to improve watermark robustness while maintaining its imperceptibility, researchers have developed perceptual coding techniques, that exploit human visual perception, and in particular the masking effect typical of the human visual system, specifically the masking effect. Masking refers to our decreased ability to perceive a stimulus (e.g., a watermark) in the presence of other signals (e.g., polygonal mesh). In the areas of image and video watermarking, various attempts have been made by utilizing luminance and frequency sensitivity, and contrast masking to improve the imperceptibility and robustness of watermarks [4], [5], [6], [7], [8], [9]. 2D Watermarking techniques taking into account human sensitivity to luminance, frequency and contrast are more effective at improving both *robustness* and *unobtrusiveness* as compared to classic 2D watermarking schemes. It suggests that the same approach can be applied to 3D watermarking with similar expected improvements. Doing so requires that we have a way to specify human sensitivity to surface variations as a function of local geometric properties, such as 3D surface roughness.

In the present study, we introduce a new approach for adaptively adjusting 3D watermark strengths based on local surface roughness. Our work takes advantage of a recent study by Corsini et al. [10] who introduced a method to estimate surface roughness of polygonal meshes for assessing visual distortions introduced by watermarking. The present study makes several

contributions. First, we quantify human sensitivity to surface variations as a function of estimated local roughness by conducting psychovisual experiments. The result is a precise functional relationship between local roughness and the Just Noticeable Difference (JND). Our approach is therefore more perception based as compared to previous attempts [11] that used the local characteristics of 3D models to adapt watermark strengths without employing human sensitivity functions.

Second, using the experimentally-derived JND vs. local roughness relationship, we propose a roughness-adaptive method for selecting 3D watermark strength that ensures locally maximal watermark strength (to improve watermark robustness) while maintaining the watermark's imperceptibility. Third, we evaluate our roughness-adaptive 3D watermarking approach by applying it to two existing 3D watermarking techniques, one proposed by Benedens [1] and the other by Cayre & Macq [2], and demonstrate the effectiveness of our approach. We also introduced several modifications and improvements to Benedens's and Cayre & Macq's methods in order to improve the methods themselves and to make them receptive to our roughness-adaptive 3D watermarking approach.

The remainder of this paper is organized as follows. In the next section, we present previous work, including a review of the two existing methods used for the evaluation of our roughness-adaptive watermarking scheme. In Section III, we describe the psychovisual experiment for estimating JND as a function of local surface roughness. Section IV describes our modifications to Cayre & Macq's method. Section V presents our roughness-adaptive watermarking approach. Evaluation results appear in Section VI. Finally, we conclude the paper in Section VII.

II. PREVIOUS WORK

In this section we review previous approaches to satisfying the invisibility requirement in 3D watermarking applications.

In image and video watermarking, it is well known that visual masking effect can be utilized in order to minimize visual distortion introduced by watermarks while maximizing watermark strengths and hence improve robustness[4], [6], [9], [7], [5]. As an extension to polygonal meshes, Ferwerda et al. [12] analyzed how the presence of one visual pattern affects the detectability of another. They demonstrated that the pattern of 3D textures can be flexibly selected and used to mask faceting artifacts caused by polygonal tessellation of a curved surface. This fact has encouraged researchers working in 3D watermarking to exploit the masking effect in several ways.

Kanai et al. [13] exploited the fact that the human vision system (HVS) is less sensitive to changes in high frequency areas of polygonal meshes. They analyzed an input mesh with a wavelet transform and modulated the high frequency components to embed the watermarks. Similarly, Bors et al. [14] used human detection thresholds on local mesh variations to choose the surface regions where the human eye is less sensitive to changes. Only those chosen vertices were then modified by the watermarks.

The key differences between our method and the above two methods are that both Bors et al. and Kanai et al. used a constant watermark strength in surface areas where humans are less sensitive to watermark embedding, and neither method embedded watermarks in surface areas where humans are more sensitive to changes. These methods therefore adapted watermark strengths in a coarse way (either on or off) without fully exploiting the way the HVS perceives watermarks. On the contrary, our method allows a continuous optimization of watermark strengths on a vertex by vertex basis.

In a study that somewhat resembles our approach, Uccheddu et al.[11] applied masking effect of surface roughness to a wavelet-based 3D watermarking method, which was previously developed by the same authors [15], to diminish the degradation of the host mesh. In the beginning stage of watermark embedding process, the host signal is decomposed in a multiresolution framework with wavelet coefficients representing surface details by means of the algorithm proposed by Lounsbery et al. [16]. Subjective experiments were conducted to estimate watermark detection threshold as a function of local roughness values. Watermarks were embedded by modifying the wavelet coefficients at a given level of resolution. Triangles to be modified were selected by using the experimentally-derived roughness-based threshold; only those vertices for which the local roughness was greater than the threshold were watermarked.

Despite the apparent similarity between our present study and that of [11], there are several important differences, concerning how watermark strength is selected and which surface areas are chosen for watermarking. In our approach, the watermark strength is selected automatically based on a human perception curve determined by psychovisual experiments, while in [11] the strength was adjusted manually. In addition, our method [17] allows watermark strength to be adjusted on a continuous scale on a vertex by vertex basis, while in [11] each vertex was either modified with a fixed-strength watermark or it was not altered at all.

The present study extends and generalizes the approach described in our previous research[17]. In the previous study, the basic idea was to adjust watermark strength according to the local surface roughness. The idea was then applied to Benedens's watermarking method [1], showing improvements in terms of roughness and invisibility. The novelties introduced in the present study includes: i) refinement of the psychovisual experiments to take into account several types of watermarking disturbances; ii) a more rigorous definition of the functional relationship between admissible watermark strength and surface roughness; iii) application of roughness-adaptive watermarking to Cayre & Macq's method whose characteristics are somewhat complementary to those of Benedens's algorithm; and iv) evaluation of the results on a larger number of 3D models.

A. Overview of two watermarking schemes

Throughout our research we considered two different 3D watermarking schemes with complementary characteristics: one developed by Benedens [1] and the other proposed by Cayre & Macq [2]. As it will become evident in this paper, these two schemes introduce quite different disturbances to

the original meshes, hence permitting us to evaluate the performance of roughness-based watermarking scheme under different conditions. In the remainder of this section, give a brief overview of these two watermarking schemes, and describe a few modifications we introduced in order to make the two methods more receptive to roughness-based adaptation of watermark strength.
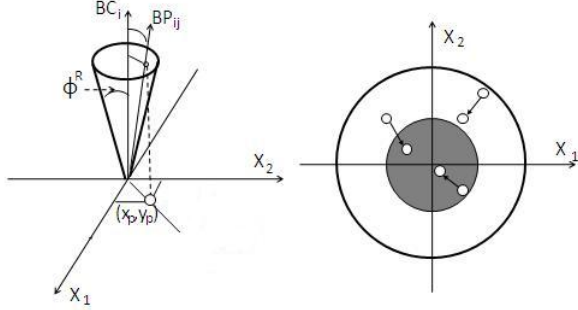

Figure 1: (left) Transformation of 3D coordinates into 2D coordinates. (right) Embedding a bit '0' by pushing normals into the kernel area. Modified from [1].

1) Benedens's method: Benedens's non-blind, geometry-based 3D watermarking method [1] uses the distribution of face normals on polygonal meshes for watermark embedding. In Benedens's method, the watermark is embedded by modifying any of the following three features: (i) the mean of normals, (ii) the mean angle of normals to a Bin Center (BC) normal, or (iii) the amount of normals in a bin. In this work we considered the third feature since it provides the most straightforward way to adjust watermark strength. Considering only the third feature, the embedding process of Benedens's method is summarized below:

1) Create a unit sphere, and then tessellate the surface of the unit sphere to generate bins defined by a Bin Center (BC) normal and a bin angle (φ^R) (also referred to as bin radius). The same bin radius is used for all the bins. Bins are cone-shaped as illustrated in the left image of Figure 1.
2) Randomly choose a set of bins for embedding watermark bits and for sampling face normals. A face normal is assigned to a bin if the angle formed between the face normal (BP) and the BC normal (Figure 1, left image) is smaller than that formed between the cone's axis (i.e.,BC) and any line on the face of the cone that passes through its apex.
3) For each bin, compute the ratio of normals (nk_i) inside the bin kernel pre-defined by a kernel angle φ^k over all normals inside the bin. The 2D projected kernel area is shown as the gray inner circle in the right image of Figure 1.
4) Transform the 3D face normals in each bin into 2D coordinates in the X_1 and X_2 plane (see the left image of Figure 1) and perform the core embedding process as described below.

During the core watermark embedding process, watermark bits are inserted by changing the number of normals inside

the kernel area in each bin. For instance, to embed a bit '0', all the normals outside the kernel are moved inside the kernel as depicted in the right image of Figure 1. It means that nk_i (the ratio of normals inside the kernel) becomes 1.0, which is the maximum for any bin. Conversely, a bit '1' is embedded by taking all the normals inside the kernel out of the kernel so that nk_i goes to 0.0, the minimum for any bin. Finding the best normal direction for embedding is performed by an optimization algorithm called the Downhill simplex method which is also called the Nelder-Mead method [18]. The Downhill simplex method is a nonlinear optimization technique using a simplex to approximate a local optimum of a problem with n variables. According to the optimizing process, an initial watermark strength value, flexibly chosen by the object size (see [1]), is optimized.

The two cost functions, defined in Eqns. 1 and 2 for bit 1 and 0, respectively, are used as an objective function for the optimization.

$$costs1_{f,v \to v'} = cos\left[\frac{\pi}{2}\left(\frac{cos^{-1}(<BP'_{ij}, BC_i>)}{\varphi^R_i}\right)\right], \quad S_i = 1 \tag{1}$$

$$costs2_{f,v \to v'} = \frac{cos^{-1}(<BP'_{ij}, BC_i>)}{\varphi^R_i}, \quad S_i = 0 \tag{2}$$

In order to minimize the distortions of the surface of the input model, the following constraints are imposed during the watermark embedding process:

- The normal of a face adjacent to a vertex *v* in the bin is not allowed to change by an angle that is larger than or equal to α;
- The normal of a face adjacent to a vertex *v* that is not in the bin is not allowed to change by an angle that is larger than or equal to β;
- No normal is allowed to leave its bin.

For watermarks retrieval, the information about bins (bin radius, kernel radius, the ratio of normals in each bin, and the chosen bins used in the embedding process) need to be delivered to the extraction stage. With the watermarked polygonal mesh, repeat the same steps (1 to 4) of the embedding process are repeated. Then the ratio of normals nk_i in each bin is compared with the original value of nk_i. If nk_i of the watermarked mesh is larger than the nk_i value of the original model, then the embedded watermark bit is a '0'. Otherwise, it's a '1'.

Watermarks embedded by Benedens's method are especially robust against mesh-simplification and vertex randomization, because the distribution of face normals is approximately invariant to these kinds of modifications of the polygonal meshes.

Two drawbacks of Benedens's watermarking algorithms exist: 1) the need to carry the original nk_i values to the retrieval stage, and 2) the intrinsic weakness of the "1" bits. In the present study, we used a modified version of Benedens's scheme introduced in our earlier study [17], which is briefly summarized below.

a) A blind version of Benedens's method: Retrieval of the watermarks embedded by Benedens's method requires the availability of a priori knowledge including bin radius, number of bins, and the original ratio of normals (*nk*) in the kernel of each bin. This information constitutes the secret key needed for retrieval of the watermark. Since the original values of *nk* depend on the polygonal mesh of the 3D object, Benedens's method may not be considered a truly blind watermarking technique. To eliminate the need to carry the original *nk* values to the watermark extracting stage, in [17] we proposed to use the probability distribution of normals in the kernel area of each bin. The main idea was to choose the kernel radius in such a way that, on average, the ratio of face normals inside the kernel was a fixed value. This was based on the assumption that normals are uniformly distributed over the object's surface and hence the probabilities associated with the distribution of normals correspond to area ratios. Then, the retrieved watermark bit was 0 if the *nk* value of the watermarked mesh is greater than the fixed ratio used by the embedder. Otherwise, it is 1. Therefore, all we had to do was to compute the exact kernel radius φ^k that satisfies the constraint that the ratio of normals inside the kernel area was fixed. A ratio of 0.5 was chosen so that there were equal number of face normals inside and outside the kernel.
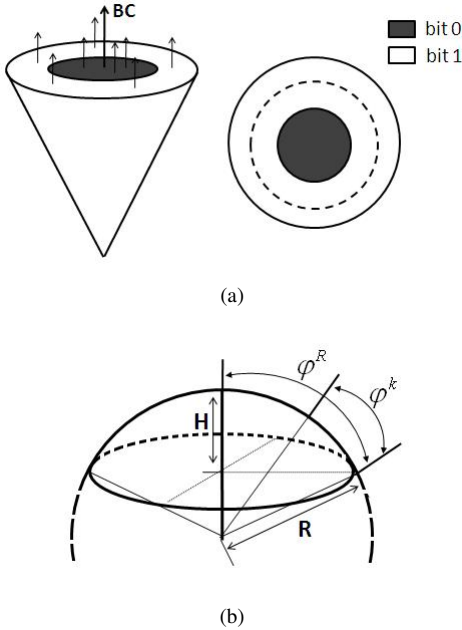

(a)

(b)

Figure 2: (a) Two views of a bin with sampled normals. The dark area (inner circle) is the kernel area defined by φ^k, which is used for embedding '0' bits. The bin area excluding the dark area is used for embedding '1' bits. The dashed circle represents the new zone for embedding '1' bits. (b) A sphere cap (a bin) defined by φ^R. R and H represent radius of the sphere and height from the top of the cap to the bottom of the base circle, respectively.

Given a spherical cap defined by a sphere of radius *R* and a height *H* (measured from the top of the spherical cap to the bottom of the base circle, see Figure 2 (b)), its surface area can be calculated as $A_{spherical\ cap} = 2\pi RH$. Since $H = R - R cos\varphi^R$ for a bin defined by φ^R, the surface area of the bin becomes

$$A_{spherical\ cap\ of\ bin} = 2\pi R^2(1 - cos\varphi^R) \qquad (3)$$

The surface area of the kernel defined by φ^k can be calculated similarly as

$$A_{spherical\ cap\ of\ kernel} = 2\pi R^2(1 - cos\varphi^k) \qquad (4)$$

We require that

$$\frac{A_{spherical\ cap\ of\ kernel}}{A_{spherical\ cap\ of\ bin}} = 0.5. \qquad (5)$$

Therefore the size of the kernel, φ^k, can be computed from Eqns. 3, 4, and 5 as:

$$\varphi^k = cos^{-1}(1 - \frac{1}{2}(1 - cos\varphi^R)). \qquad (6)$$

With this modification, the original *nk* values no longer need to be carried to the extraction stage. We have therefore achieved a blind version of Benedens's method.

b) Improvement to bit '1' robustness: In the original Benedens's method, during the embedding process, the normals are moved in two opposite directions. When embedding a bit '0', all normals in the bin are moved inside the kernel area (the dark inner circle shown in Figure 2a). For better robustness, the normals should be enforced to be as close to the BC line (bin center normal) as possible. When embedding a bit '1', however, the normals are moved towards the border of the bin and are pushed as closed to the rim of the bin as possible. There are therefore two imaginary embedding zones: one around the BC and the other around the rim of the bin. Ideally, all normals should be placed at either the BC (for bit '0') or on the rim of the bin (for bit '1'). The problem, however, is that the normals located on the rim of the bin can be easily pushed out of the bin. As a result, the embedded watermark on the bin cannot be recovered correctly at the extraction stage. This problem does not occur with the normals located at the BC. Therefore, bit 1 is less robust than bit 0 in the original Benedens's method.

To improve the robustness of bit '1', the ideal embedding zone has to be moved away from the bin rim, as shown by the dashed circle in the right image of Figure 2a. The new embedding zone defined by the dashed circle was defined by a new radius φ^{k1} such that the surface area of the spherical cap is 3/4 of that of the bin. Following Eqns. 4 to 5, we have:

$$\varphi^{k1} = cos^{-1}(1 - \frac{3}{4}(1 - cos\varphi^R)) \qquad (7)$$

With this new embedding zone for bit '1', the robustness of '1' bits is significantly improved. Overall, the robustness of '0' bits is still expected to be superior to that of '1' bits, because the new embedding zone for bit '1' is still closer to the rim of the bin than that for '0' bits.

2) Cayre and Macq's method: Cayre and Macq's method builds upon the basic idea of TSPS (Triangle Strip Peeling Sequence) that encodes a payload by moving over a triangular surface mesh. With this method, each triangle always has one entry edge and two possible exit edges as seen in Figure 3a. The watermarking algorithm requires two main steps as described below.
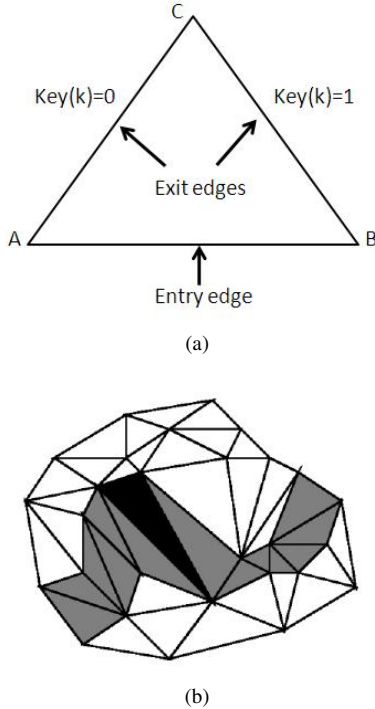

(a)

(b)

Figure 3: (a)A triangle to be traversed for watermarking by Cayre and Macq's method. (b) An example of a list of triangles generated by a secrete key. The TSPS (Triangle Strip Peeling Sequence) path is in gray and the cell to be processed is in black. From Figure 2 in [2].

1) Generate a list of triangles of the mesh: The list of triangles is established as seen in Figure 3b. The list of triangles is stored as a secret key to be carried to the extractor. The length of the key must be the same as that of the list of admissible triangles required to convey the payload.

2) Construct a Macro Embedding Procedure (MEP): Each triangle has two states defined by the position P(C) of the orthogonal projection of the triangle summit C on the entry edge AB. The entry edge AB is divided into two subsets S_1 ("1") and S_0 ("0") as seen in Figure 4b. If P(C)$\in S_0$, then the triangle is in a "0" state; otherwise, P(C) $\in S_1$, and the triangle is in a "1" state. For every triangle, there are two possible cases: (1) P(C)$\in S_i$, and no modification is needed; or (2) P(C) $\notin S_i$, then C is move to C' so that P(C')$\in S_i$(see Figure 4b), where i is 0 or 1.

The value of λ(seen in Figure 4b) has to be small enough to avoid visual degradation of the mesh, but large enough to allow accurate payload detection. The parameter n (see Figure
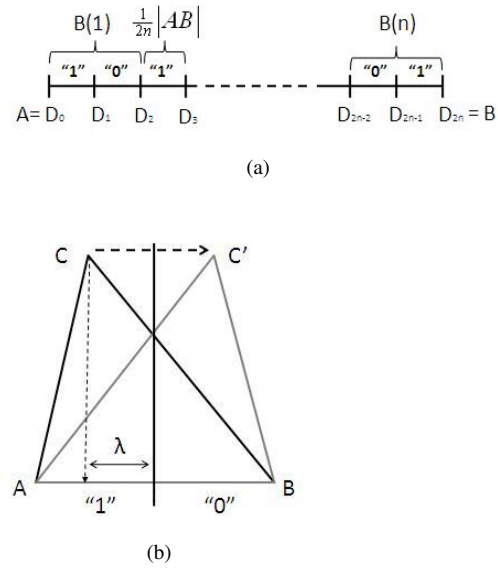

(a)

(b)

Figure 4: (a) Decomposition of the entry edge AB into two interleaved subsets with the 2n binary values. (b) An example of the first-order MEP (Macro Embedding Procedure, n=1) encoding. Modified from Figure 4 [2].

4a) represents the smoothness of the algorithm. As n increases, λ decreases and the amount of distortion to be introduced gets smaller. On the other hand, as n increases, bit retrieval errors also increase due to the decrease in the interval size. This leads to reduced robustness.

III. WATERMARK PERCEPTIBILITY AS A FUNCTION OF SURFACE ROUGHNESS

In this section, we present the psychovisual experiment that we designed and carried out to derive the functional relationship between local surface roughness and the maximum watermark strength that can be used while maintaining watermark invisibility. Specifically, human detection thresholds for the perceptibility of geometrical surface distortions were estimated for three watermarking techniques: Benedens's method, Cayre & Macq's method, and watermarks consisting of the additive Gaussian noise to vertex positions. It was conceivable that the threshold curves for the three methods would be quite different since the strategies to embed watermarks are all different. If this turned out to be the case, then a different rule should be used to adjust watermark strength according to the watermarking method. On the other hand, if the threshold curves were similar for the three watermarking techniques, then the same adaptation rule could be used regardless of the watermarking technique.

The three different methods were selected because they differ in the directions along which vertices are modified with respect to the normals of surface mesh. Benedens's method perturbs vertex normals by changing the locations of the vertices that belong to a bin with a radius ϕ (see Figure 5a). The direction of the vertex change is the same as the direction of normal change. The range of allowable changes is limited by the size of the bin radius ϕ. The distortion made by Cayre

& Macq's method, on the contrary, is made in a direction perpendicular to the normal of a triangular mesh (see Figure 5 b). The new vertex C lies on a line parallel to the triangle edge AB. In this case, the normal N is always preserved during the perturbation. Using additive Gaussian noise, a vertex is changed in a randomized direction (see Figure 5 c).

In summary, both Benedens's method and additive Gaussian noise alter the normals of triangular meshes whereas Cayre & Macq's method does not. Additive Gaussian noise can also result in larger distortions than Benedens's method since changes to the vertex (C in Figure 5) is unlimited in its direction. Therefore, we were interested in comparing human threshold curves for Benedens's method and additive Gaussian noise, as well as comparing the curves for these two methods to that of Cayre & Macq's method.
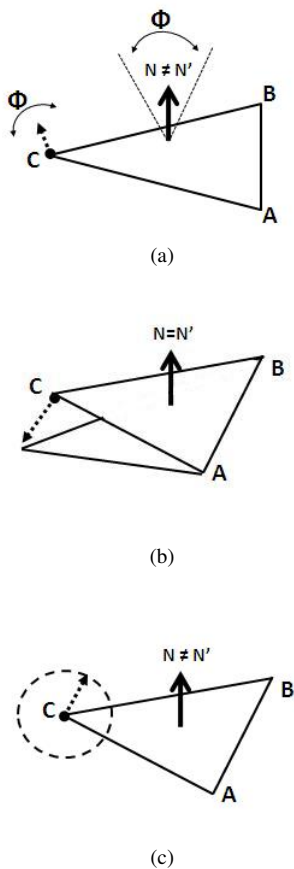
(a)

(b)

(c)

Figure 5: Three different strategies for watermark embedding on a triangle. N are N' are normals before and after distortion. (a) Geometrical change of a triangle by Benedens's method with a bin radius ϕ. (b) In plane vertex distorted by Cayre & Macq's method. (c) Watermarking with additive Gaussian noise. The dashed circle around the vertex C represents the projection of a sphere for the range of allowable changes.

A. Methods

The psychovisual experiment was designed to estimate the relation between visual watermark detection threshold (in terms of watermark strength δ) and local roughness of

spherical surfaces. The watermark strength δ is controlled differently in the three watermarking methods since the geometrical properties used for watermarking are different. For instance, in Benedens's method control of watermark strength is obtained by restricting the search space in the Downhill Simplex optimization method based on the minimum of four parameters including δ. In Cayre & Macq's method, watermark strength is not easily modifiable since it is affected by the partition size determined by the order of MEP. We therefore modified the original Cayre & Macq's method to make the watermark strength easily modifiable for our experiments (See details in Section IV). The watermark strength δ for additive Gaussian noise method corresponds to the amount by which a vertex is altered in a randomized direction. In the present study, δ is expressed as a normalized value over the diagonal length of the bounding box of a 3D object.

B. Participants

Ten participants (five males and five females) took part in the experiment. None of the participants reported any visual deficiencies.

C. Stimuli

The visual display consisted of a spherical surface rendered with 3752 vertices and 7500 faces. The image of the sphere occupied a visual angle of roughly 30 degrees. Five reference spherical surfaces with different roughness levels were created. Roughness was controlled by perturbing the vertices with additive Gaussian noise. Specifically, the roughness level was specified by the variance of a Gaussian probability distribution function $N(0,\sigma)$ that generated the additive noise. The direction of the additive noise was chosen randomly. Figure 6 shows the five reference stimuli with increasing surface roughness. The left-most sphere has a smooth surface with no additive noise. The roughness level of each spherical surface was estimated with a 1-ring roughness measure based on the multi-scale roughness estimation method proposed by Corsini et al. [10]. The estimated roughness for the five reference surfaces were 0.000082, 0.001704, 0.003139, 0.010937 and 0.025304, respectively.

Figure 6: . The five reference spherical surfaces used in the present psychovisual experiments. The estimated roughness values were, from left to right, 0.000082, 0.001704, 0.003139, 0.010937, and 0.025304, respectively. The five surfaces contained the same number of vertices (3752) and faces (7500).

Each of the three watermarking schemes was applied to each of the five reference surfaces to obtain human detection thresholds for visual watermarks. Due to the time required to generate watermarked surface using Benedens's method, the stimuli for Benedens's method were pre-computed. The stimuli

for the other two watermarking methods were computed in real time.

The parameters used for the Benedens's method were $\varphi^R = 10$ degrees, 10 bins, and no β. For Cayre & Macq's method, a list of triangles was randomly generated for embedding the watermark and the vertices of the list of triangles were altered by the modified version of Cayre & Macq's method for roughness adaptation (see also section IV).

For the watermarking method using additive noise, Gaussian noise was used to randomly alter chosen vertices of the spherical surface in a random direction, as specified below:

$$\overrightarrow{v}_{new}(i) = \overrightarrow{v}(i) + \delta * \overrightarrow{n_r}(i)$$

where $\overrightarrow{v}_{new}(i)$ is the modified vector of the i-th vertex $\overrightarrow{v}(i)$, δ denotes the watermark strength that varied according to the correctness of participant's responses, and $\overrightarrow{n_r}(i)$ is a random unit normal vector.

D. Procedures

A three-interval forced-choice (3IFC) one-up one-down adaptive procedure [19] was used to measure watermark detection thresholds as a function of surface roughness. The threshold so obtained corresponded to the 50 percentile point on the psychometric function. On each trial, the participant looked at three spherical surfaces, two reference surfaces (without watermarks) and a test surface (with watermarks), presented on a computer monitor. The position of the watermarked surface was randomly chosen to be on the left, middle, or right of the monitor on each trial. The participant's task was to indicate which spherical surface looked different (i.e., contained the watermark). According to the one-up one-down adaptive rule (see Figure 7), the stimulus intensity (δ) was increased after an incorrect response and decreased after a correct response. The initial δ value was chosen to be large enough so that the test surface looked clearly different from the reference surface. The value of δ then decreased or increased by a fixed step size (6dB), depending on the participant's responses. After three initial reversals (a reversal occurred when the value of δ decreased after increasing, or vice versa), the value of δ changed by a smaller step size (2dB). The initial larger change in δ was necessary for faster convergence of the δ values, whereas the later smaller change in δ improved the resolution of threshold estimates. The adaptive series was terminated after 12 reversals at the smaller step size. The detection threshold was computed by taking the average of the δ values from the last 12 reversals. Each participant was tested once per combination of reference surface roughness and watermarking method, resulting in a total of 15 adaptive series (5 references $\times$ 3 watermarking techniques) per participant. It took about one and a half hours for each participant to finish all the 15 series.

E. Results

The average detection thresholds for the ten participants are shown in Figure 8. For each watermarking method, thresholds followed a monotonically increasing trend as surface roughness increased. The thresholds with Cayre & Macq's method
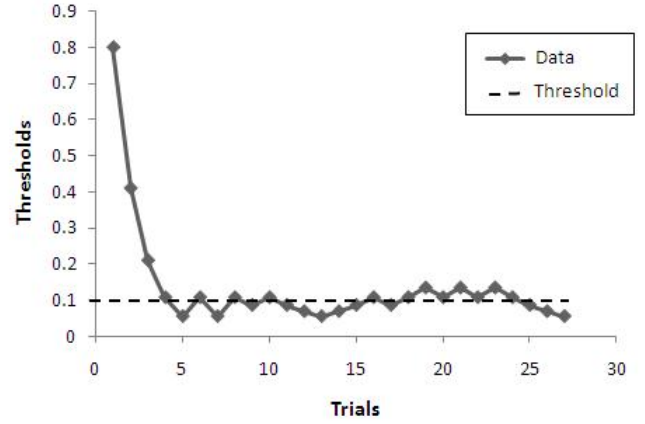

Figure 7: 1U1D(One Up One Down) Representative data plot the one-up one-down adaptive procedure. The data converge around the threshold indicated by the dashed line.

are much larger than those with Benedens's method and additive Gaussian noise, indicating that stronger watermarks can be embedded with Cayre & Macq's method. The results suggest that humans are more sensitive to changes in the direction of normals than to changes of vertices in a plane that is perpendicular to face normals. It is also apparent that the thresholds for Benedens's method and additive Gaussian noise were very similar, suggesting that the range of directions along which vertex C can be altered (see Figure 5) does not have a strong effect on the perceptibility of watermarks.

The data shown in Figure 8 were fit by power regression models with R^2 values [1] of 0.9665, 0.9841 and 0.982 for Cayre & Macq's method (CAY), additive Gaussian noise (AGN), and Benedens's method (BEN), respectively. The three best-fitting power functions are as follows:

$$\delta_{CAY} = 0.0195 * S^{0.1814} \tag{8}$$

$$\delta_{AGN} = 0.0313 * S^{0.4499} \tag{9}$$

$$\delta_{BEN} = 0.3851 * S^{0.3851} \tag{10}$$

where δ_{CAY}, δ_{AGN}, and δ_{BEN} denote watermark strengths for the respective watermarking techniques, and S denotes local surface roughness.

These results suggested that the same regression model can be used for Benedens's method and the additive Gaussian noise methods, as the best-fitting curves are quite similar in Figure 8. In the present study, we used Eqn. 10 for both the Benedens's method and the additive Gaussian method, and used Eqn. 8 for Cayre's and Macq's method. In section V, we show how the regression models shown in Eqns. (8) and (10) can be used to devise a roughness adaptive embedding rule.

---

[1]The R^2 value indicates how well a regression model approximates data points, where R^2=1.0 means a perfect fit. It is calculated by $R^2 = Cov(X,Y)/\{StdDev(X) * StdDev(Y)\}$
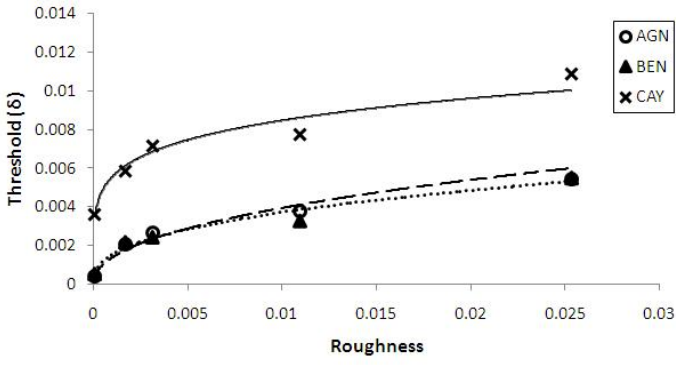
Figure 8: Power regression models of human sensitivity to watermarks for the three watermarking scheme. See texts for details.

(a) The original structure (n=1), edited from [2]

(b) Our modified structure

Figure 9: A comparison of entry edge decomposition using the original Cayre & Macq's method and our modified version.

IV. MODIFICATIONS TO CAYRE & MACQ'S METHOD

In the original watermarking algorithm proposed by Cayre & Macq, the watermark strength can not be easily controlled. The watermark strength depends on the number of intervals into which the entry edge of the triangle is split, and the derivation from the number of intervals to watermark strength is not straightforward. For this reason, we modified Cayre and Macq's method to make it suitable for the incorporation of our roughness-based watermark-strength adaptation scheme. The rest of this section describes the modifications in details.

A. New partition of the entry edge AB

The limited freedom in handling the size of watermark strength with the original entry-edge decomposition described in Figure 9a motivated us to propose a new decomposition of the entry edge AB that makes it possible to control watermark strength (see Figure 9b). The key difference from the original Cayre & Macq's method was that two infinite sized intervals (I_0 and I_3) were added to increase watermark strength, thereby guaranteeing improved watermark robustness. The entry edge AB is extended in both directions into infinitely and divided into four intervals by D_0, D_1 and D_2 (see Eqn. 11) as seen in Figure 9b.

$$I_{k+1} = \overline{D_k D_{k+1}}, \ for \ k = 0, 1$$
$$|I_{0 \, or \, 3}| = \infty \ \& \ |I_{1 \, or \, 2}| = \tfrac{1}{2}|AB| \qquad (11)$$
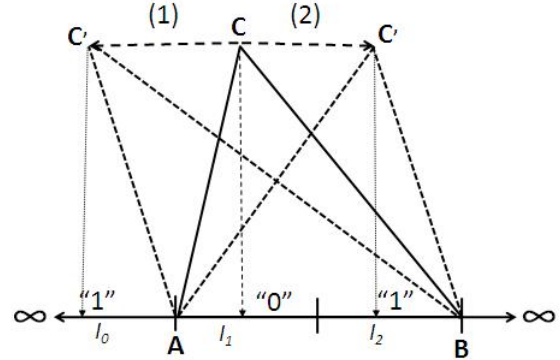
B. Embedding

With our modified decomposition method, the position of the vertex C' (see Figure 4) was changed for both cases of $P(C) \notin S_i$ and $P(C) \in S_i$. Recall that the original Cayre and Macq's method allows a symmetrical reflection of vertex C to C' only when $P(C) \notin S_i$. Eqn. 12 shows how the new position of the vertex C' was calculated in our modified method:

$$C' = C + \delta_{est} \cdot \overrightarrow{N} \qquad (12)$$

where C and C' were the current and new vertices, δ_{est} determines the watermark strength (see Eqn. 15 later in Section V), and $\overrightarrow{N} = C' - C$ is a unit vector parallel to the AB edge.
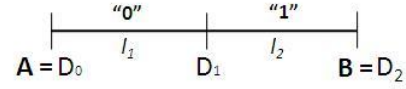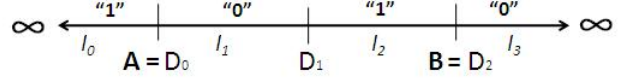
Figure 10 further illustrates how vertex C should be modified in both cases $P(C) \notin S_i$ and $P(C) \in S_i$. For simplicity, we discuss the embedding of bit '1', since the extension to bit '0' is trivial. Watermarks can be embedded in two different ways, hereafter called method (1) and method (2), respectively. By referring to Figure 10, method (1) enforces C to move toward a position C' which belongs to B_0 of infinite size, whereas method (2) moves C toward a position C' in B_2 of a limited size.

(a) when P(C) ∉ S$_i$
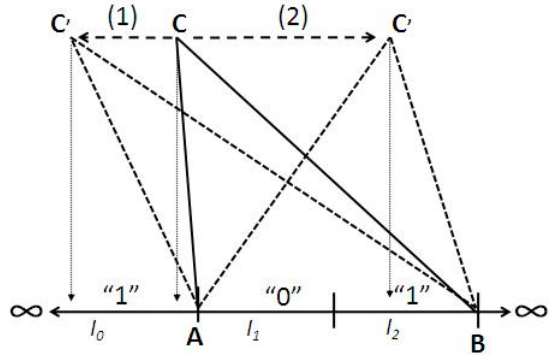
(b) when P(C) ∈ S$_i$

Figure 10: Two examples of embedding. For each example, two candidate directions exist for the modification.

Although a modification can occur by either method (1) or

(2) depending on the value of δ_{est} (see Figure 10), method (1) is more desirable. This is because B_1 and B_2 are of equal sizes and divide the length of AB evenly, whereas B_0 and B_3 are of infinite size and extend from A and B towards infinity, respectively. If C can move further in B_0 towards infinity, then a superior robustness is obtained since it becomes much harder for an attack to push C' out of B_0. Watermark strength δ_{est} is determined according to the results of the psychovisual experiments. More specifically, the modified version of Cayre and Macq's method can be summarized as follows.

1) Generate a list of triangles of the mesh: The list of triangles is established as seen in Figure 3b. The list of triangles is stored as a secret key to the extractor. The length of the key must be the same as that of the list of admissible triangles required to convey the payload.
2) Create a new edge decomposition as seen in Figure 9b.
3) Perform the core embedding process as follows: (1) when $P(C) \in S_i$, the position of vertex C is modified, and it either remains in the same interval or it moves into the other interval belonging to the same S_i set. (2) When $P(C) \notin S_i$, the vertex C is moved into one of two intervals that do not belong to the S_i set (see Figure 11). Further details of this core embedding step are explained below.
4) Repeat step 3 until all the triangles on the list have been traversed.

(a) when P(C) falls into I_0, $P(C) \notin S_i$

(b) when P(C) falls into I_1, $P(C) \in S_i$

(c) when P(C) falls into I_2, $P(C) \notin S_i$

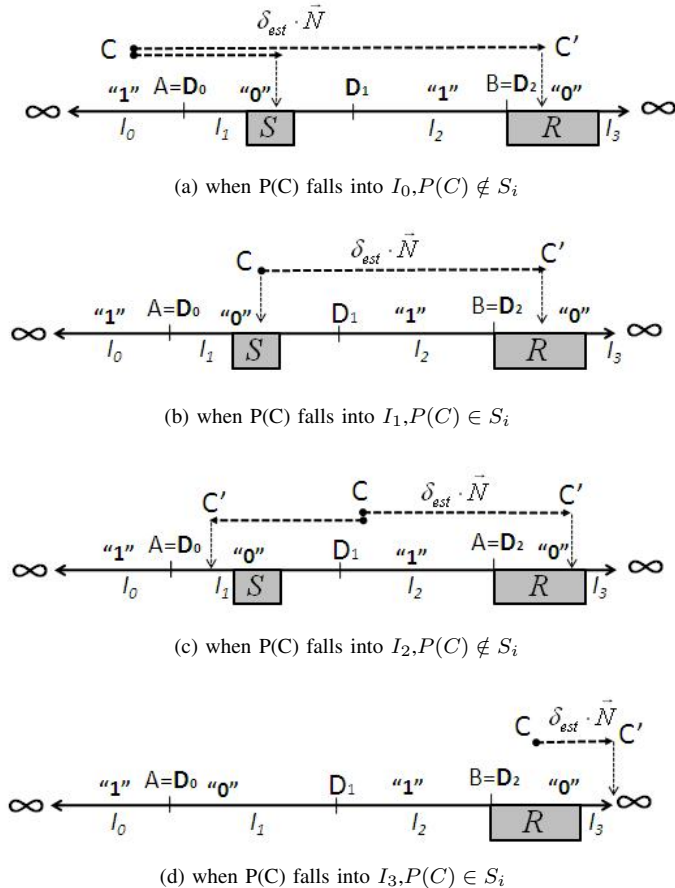(d) when P(C) falls into I_3, $P(C) \in S_i$

Figure 11: Examples of core embedding process when $S_i = 0$. Only relevant S and R are marked.

Figure 11 illustrates further details of the aforementioned step 3. For each interval defining I_0, I_1, I_2 and I_3, safe (S) and risky (R) zones are defined as depicted in Figure 11. The size of these zones are as follows:

$$\begin{aligned} \overline{S} &= \tfrac{1}{3}|I_k|, \quad for\ k = 1\ or\ 2 \\ \overline{R} &= \tfrac{1}{2}|I_k|, \quad for\ k = 1\ or\ 2 \end{aligned} \qquad (13)$$

An S zone is always located at the center of I_1 or I_2, whereas a R zone is located at the (non-infinite) border of I_0 or I_3. When the embedder has to decide the new position for vertex C, it prefers S zones and tries to avoid R zones. Specifically, let us consider again the case of a '0' bit, i.e. $S_i = 0$. Four possible cases can occur during watermark embedding.

In the first case. P(C) falls in I_0 (see Figure 11a). In this case, the embedder determines whether C moves to I_1 or I_3 since $P(C) \notin S_i$. With a given watermark strength δ_{est}, the embedder tries to reach I_3 while avoiding R. If this is not possible, the embedder moves C' into I_1, possibly by using a δ that is lower than the originally estimated one (δ_{est}). Note that when C is moved into I_3, C' can be moved as far away from C as possible within I_3. On the contrary, when C' is moved into I_1, its optimum position is to be as close to the center of I_1 as possible (i.e., the S zone). However, the allowable distortion (δ_{est}) may prevent C' from being moved into the S zone. move C into the safe zone S. In an even worse situation, it may be impossible to move C outside of I_0 if δ_{est} is very small (e.g., zero roughness). This issue was resolved by adding a correction function which moves C into I_0 or I_3 by recomputing δ_{est} when the value of roughness is zero. The correction function assigns a value of δ_{est} in order to allow C be moved into I_0 or I_3 while avoiding the R zone. Note that the magnitude of δ_{est} can be any value since perturbation occurs on a flat surface (see Figure 5b).

In the second case, $P(C) \in S_i$ and P(C) falls into I_1 (see Figure 11b). The embedder tries to move to C to I_3 first by avoiding R. If it is successful, embedding is complete, otherwise the embedder tries to move C as close as possible to the center of I_1.

In the third case, $P(C) \notin S_i$ and P(C) falls into I_2 (see Figure 11). In this case the embedder first tries to move C toward B_3, if it fails, it tries to move C into the S region of I_1. Both are failed, the vertex C chooses the closest one of two intervals to move in by comparing two euclidean distances, from C to I_1 and to I_3, respectively.

In the last and simplest case, there is only one direction for the vertex C to move within the interval I_3 to improve robustness (see Figure 11d).

As explained above, it is sometimes necessary to reduce watermark strength during the embedding process in order for C' to be in an S region. As a result, there is a discontinuity in the way the embedder can control the watermark strength as a function of local surface roughness.

V. ROUGHNESS ADAPTIVE WATERMARKING

By relying on the results of the psychovisual experiment described earlier, we now propose an adaptive approach to

select watermark strength based on local surface roughness measures. Our algorithm takes advantage of the fact that the human eyes are more sensitive to distortions of smoother surface patches than to distortions of rougher surface patches. Indeed, the results of the psychovisual experiment indicated that a stronger watermark can be hidden into a bumpier surface area with a higher roughness level. Specifically, the watermark detection threshold for watermarks increases monotonically with the local surface roughness as shown in Eqn.8, 9, and 10. Our goal is to use an adaptive watermark strength determined by the local surface roughness instead of the constant watermark strength used in Benedens's method and Cayre & Macq's method. While satisfying the imperceptibility constraint, our method will result in a higher average watermark strength, that will lead to an improved robustness. Our proposed algorithm works as follows. The embedder first estimates the roughness level at each vertex. It then chooses the maximum imperceptible watermark strength using Eqns. 14 and 15:

$$\delta_{BEN} = \begin{array}{ll} 0.3851 * S^{0.3851} & for\ S \geq 0.000082 \\ 0.0001 & for\ S < 0.000082 \end{array} \tag{14}$$

$$\delta_{CAY} = \begin{array}{ll} 0.0195 * S^{0.184} & for\ S \geq 0.000082 \\ 0.001 & for\ S < 0.000082 \end{array} \tag{15}$$

where S denotes surface roughness. Recall that the surface roughness of the smoothest spherical surface used in the psychovisual study (See Figure6) was 0.000082. For smoother surface with roughness values lower than 0.000082, we have heuristically set the watermark strength to a constant. In practice, however, we rarely expect to encounter a surface roughness value as low as 0.000082 for most 3D surfaces.

To estimate the local surface roughness around a to-be-modified vertex, the embedder estimates the roughness of all adjacent faces around the vertex using the 1-ring roughness estimation method described in Corsini et al. [10]. The value of δ is then determined by Eqn. 14 or 15 for the modified Benedens's method or the modified Cayre & Macq's method, respectively.

VI. PERFORMANCE EVALUATION OF ROUGHNESS-BASED ADAPTIVE WATERMARKING

To evaluate the validity of the roughness-adaptive 3D watermarking approach, we applied it to the modified versions of Benedens's method and Cayre & Macq's method. We focused on investigating how robustness was improved by our roughness-adaptive strategy. Attacks were simulated by additive noises generated with a Gaussian distribution and all of the surface vertices were altered by the noise. The performance levels of our improved methods and those of the original methods were compared in terms of robustness against additive noises. Note that imperceptibility was ensured for all 3D models used and all watermarking methods considered.

A. 3D Models

Six 3D models, "Angel (M1)", "Bunny1 (M2)", "Bunny2 (M3)", "Dragon (M4)", "Gorilla (M5)" and "Happy Buddha (M6)", were used for the evaluation experiments. The key characteristics of the six models are summarized in Table I. As it can be seen, the models differ in terms of resolution and surface roughness. It is expected that models with larger variations in roughness values will benefit more from our roughness-adaptive watermarking approach. The watermarked models after roughness-adaptive watermarking are shown in Figure 12.

Table I: Key parameters of the six 3D models used in the present study

Model	# of Vert.	# of Faces	Avg. Roughness	Std. Dev.
M1	5002	10000	6.51E-08	4.64E-08
M2	5050	9999	1.89E-07	1.75E-07
M3	7525	14999	7.34E-08	8.50E-08
M4	3512	6999	1.33E-06	8.84E-07
M5	7521	14999	2.97E-08	2.84E-08
M6	4952	9932	7.52E-07	4.48E-07
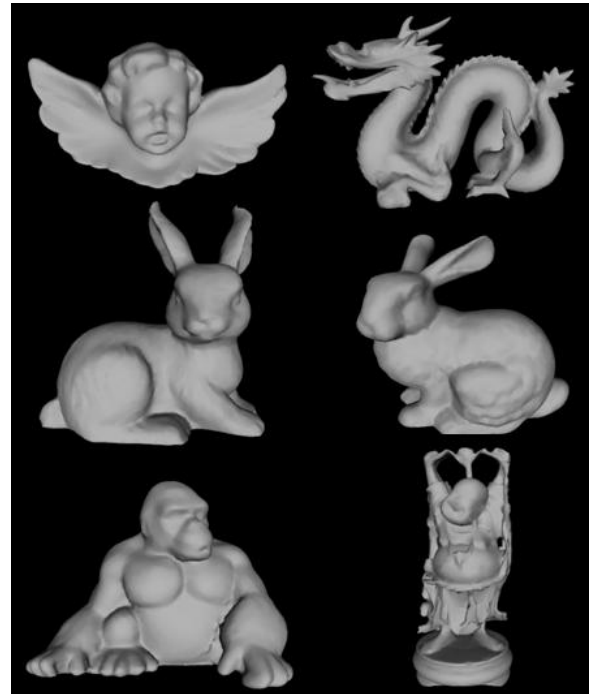
Figure 12: Watermarked models resulting from by our roughness-adaptive approach: Angel and Dragon (first row), Bunny2 and Bunny1 (second row), and Gorilla and Happy Buddha (third row).

B. Roughness adaptive watermarking of the 3D models

Table II: Experimental Conditions

Experimental Condition	Watermarking Method	Watermark Strength δ
I	Modified Benedens	constant
II	Modified Benedens	adaptive
III	Cayre & Macq	variant but not adaptive
IV	Cayre & Macq	adaptive

The evaluation experiments were considered with four conditions as seen in Table II. For Condition I, the modified Benedens's method with improved robustness of '1' bit and blindness was used with a constant watermark strength δ. The constant δ value was chosen from a pilot test where the maximum δ value averaged from five repetitions was selected for imperceptible watermarking with each 3D model. Condition II used the same modified version of Benedens's method with our roughness adaptive scheme. In this condition, δ was adaptively selected based on local surface roughness during the embedding process. Condition III used Cayre & Macq's method where watermark strength was determined by the type of triangles and by the order of MEP (n=2). In other words, δ size varied with each of the triangles on the list of triangles to be modified and was not optimized during the embedding process. In Condition III, the δ value for each triangle was recorded and averaged to be compared with the δ values by our roughness-adaptive approach (i.e., Condition IV). Condition IV was the roughness-adaptive version of the modified Cayre & Macq's method, where δ values were adaptively selected according to local surface roughness (see also Section IV).

For Conditions I and II, the relevant parameters were set as follows: φ^R = 10 degrees, $\alpha = 10$ (heuristically chosen), 20 bins (i.e., 20 watermark bits), no β, and the entire embedding process was reiterated twice in order to get a refined δ value during the embedding process. The difference between Condition I and II was related to the need of the initial watermark strength δ before starting the embedding process. For Condition I, the initial δ value was chosen by a pilot study ensuring imperceptibility. For Condition II where our roughness-adaptive approach was employed, the δ value was adaptively selected by applying Eqn. 14 to the measured local surface roughness value.

To test robustness, Gaussian random noise (N(0, σ=0.0005)) was added to the watermarked model in order to randomly alter the locations of all vertices in the model. The bits of the embedded watermarks were then extracted and compared with the original ones. Error rate was computed in terms of the percentage of mismatched bits. The experiment with each method was repeated ten times. With each iteration, a new set of Gaussian noise, watermark bits and bins to be watermarked was selected randomly.

For Conditions III and IV, a list of about three hundred triangles was randomly generated for each model. The order of MEP was experimentally chosen over all six models for Condition III because the MEP's order determined the interval size for the decomposition of each triangle, which affected the amount of actual visual distortions. During the embedding process for both Conditions III and IV, the magnitudes of the modification introduced by the watermarking process for each triangle were recorded and averaged for each 3D model. The robustness evaluation was conducted in the same way as with the modified Benedens's method. The experiments were also repeated ten times for each 3D model.

C. Procedures

Watermarking methods were implemented using C++ with CGAL and OpenGL libraries for PCs running the Windows environment. Five PCs with processing speed from 2.4 GHz to 3 GHz were used. Each PC was equipped with a 17" TFT PC monitor. The 3D models were graphically displayed using the Gouraud shading technique [20]. On each PC, watermarks were embedded to one of the models under all four conditions. The robustness of the watermarks was then evaluated with respect to the addition of Gaussian random noises. The procedure was then repeated for all six models.

D. Results

Table III: A comparison of watermark decoding errors due to additive-noise attacks for the modified Benedens's method (Condition I and II). The average and the standard deviation of the error rate for each model are shown for each condition. The improvement is shown as the reduction in error rate in percentage.

Model	Condition I (%)	Condition II (%)	Improvement (%)
M1	10 ± 3.16	4.5 ± 3.69	55.0
M2	9.5 ± 3.50	4 ± 2.11	57.9
M3	9 ± 3.74	4 ± 3.16	55.5
M4	10 ± 3.47	2.5 ± 2.64	75.0
M5	9.5 ± 2.69	4.5 ± 2.84	52.6
M6	9.5 ± 4.15	3.5 ± 2.42	63.2

Table IV: A comparison of watermark decoding errors due to additive-noise attacks for Cayre and Macq's method (Conditions III and IV). The average and the standard deviation of the error rate for each model are shown for each condition. The improvement is shown as the reduction in error rate in percentage.

Model	Condition III (%)	Condition IV (%)	Improvement (%)
M1	42.9 ± 1.49	23.3 ± 3.49	45.6
M2	48.3 ± 4.58	22.8 ± 3.41	52.6
M3	47.4 ± 2.85	24.5 ± 4.52	48.8
M4	46.8 ± 4.67	18.0 ± 1.93	61.6
M5	45.5 ± 2.48	24.1 ± 2.58	46.9
M6	44.0 ± 3.15	19.6 ± 3.67	55.5

Table V: A comparison of watermark strengths for the modified Benedens's method and (Conditions I and II). All values are scaled down by 1000.

Model	Condition I	Condition II	Improvement (%)
M1	1.14 ± 0.13	2.06 ± 0.48	80.4
M2	1.05 ± 0.066	2.65 ± 0.57	151.7
M3	1.06 ± 0.022	1.98 ± 0.65	85.45
M4	1.29 ± 0.098	8.21 ± 0.79	534.8
M5	1.09 ± 0.086	1.94 ± 0.88	77.5
M6	1.03 ± 0.014	4.79 ± 0.64	364.9

The results of the evaluation experiments are shown in Tables III (for Conditions I and II) and IV (for Conditions III and IV). It is clear that watermarks embedded by using our adaptive δ method (Conditions II and IV) are more robust

Table VI: A comparison of watermark strengths for Cayre and Macq's method (Conditions III and IV). All values are scaled down by 1000.

Model	Condition III	Condition IV	Improvement (%)
M1	1.15 ± 0.21	4.64 ± 0.35	300.2
M2	1.17 ± 0.71	4.88 ± 0.48	318.9
M3	1.17 ± 0.10	4.78 ± 0.49	309.2
M4	1.16 ± 0.59	5.90 ± 0.97	409.6
M5	1.12 ± 0.27	4.49 ± 0.37	302.4
M6	1.20 ± 0.26	5.73 ± 0.39	357.1

against additive-noise attacks for all the six models. The robustness improvements achieved by our method (Condition II) from the modified version of Benedens's method ranged from 52.6% with the Gorilla (M5) to 75% with the Dragon model (M4). The improvements in robustness over Cayre & Macq's method ranged from 45.6% with the Angel model (M1) to 61.6% with the Dragon model (M4) (see Table IV). As expected, the largest improvement occurred with the Dragon model because the standard deviation of surface roughness for the Dragon model (M4) was the largest among the six models tested (see Table I).

It was also found that the average value of δ was larger with our roughness-adaptive methods (Conditions II and IV) than with the modified Benedens's method (Condition I) and Cayre's & Macq's method (Condition III). The increase in δ was greater with the Dragon model (M4) and the Happy Buddha model (M6) than that with the other models (see Table V and Table VI). Therefore, as we expected, the models with the larger variations in surface roughness (the Dragon model) benefited more from our roughness-adaptive method.

E. Discussions

We focused our assessment by comparing the watermark strengths between the non-adaptive and adaptive methods (Condition I vs. II, and Condition III vs. IV, respectively). From our results (Tables III, V, IV and VI), it can be clearly stated that roughness adaptive watermarking employing human sensitivity to local surface roughness significantly improves overall watermark strength, leading to superior robustness against attacks. The results with both Benedens's method and Cayre and Macq's method strongly support the statement although the impact of the roughness-adaptive watermarking approach varies with the characteristics of input models, with models having larger surface roughness variations benefiting more from this approach.

As seen in Tables V and VI, overall δ was increased more with Cayre & Macq's method than with Benedens's method. One reason for this difference is that people are more sensitive to perturbations with Benedens's method (hence a lower watermark detection threshold) than with Cayre & Macq's method (see Figure 8). As a result, the watermark embedder was able to increase watermark strength more with Cayre & Macq's method when utilizing the roughness-adaptive approach. Another reason is that the maximized δ values in the case of zero surface roughness with Cayre & Macq's method contributed to a further increase of the overall watermark

strength as compared to Benedens's method. An exception to this general trend is found in the forth row (M4: Dragon model) of Tables V and VI, where the increase in watermark strength with Benedens's method is larger than that with Cayre and Macq's method. The reason is that the constraint of the modified Cayre and Macq's method (discontinuity of watermark strength described at the end of Section IV) resulted in a reduction of the maximized watermark strength that could be achieved with the modified Benedens's method (Condition II).

VII. CONCLUSIONS

Developing robust 3D digital watermarking techniques is an ongoing challenging research topic in the field of information hiding. In this paper, we have presented a general way to improve watermark robustness by exploiting masking effects of human visual perception. Our method is based on a measure of human sensitivity to surface variations as a function of surface roughness of input meshes.

The evaluation experiments in which we applied our roughness-adaptive scheme to two existing 3D watermarking methods by Benedens and by Cayre and Macq confirmed that the overall watermark robustness is improved significantly as a result of increased watermark strengths through roughness-adaptive watermark embedding. As expected, these experiments demonstrated that the roughness-adaptive watermarking technique brings about more benefits to data models with larger standard deviations of surface roughness levels. We showed that, on average, stronger watermarks can be embedded with roughness-adaptive watermark strengths than could be achieved with a constant watermark strength as used by most watermarking methods.

By combining our results with the results of Uccheddu et al. [11], we can make a general statement that utilizing masking effect due to surface roughness of polygonal meshes is an effective way to improve watermark robustness while maintaining watermark imperceptibility. Therefore, our approach suggests promising new directions for improving the performance of 3D digital watermarking schemes. In the future, we will continue to evaluate our roughness-adaptive scheme with additional 3D models. We also plan to investigate masking effects characterized by other geometric properties such as 3D curvatures. Our ultimate goal is to explore the masking property of human visual system as a general strategy for improving 3D digital watermarking techniques.

REFERENCES

[1] O. Benedens, "Geometry-based watermarking of 3d models," *Computer Graphics and Applications, IEEE*, vol. 19, no. 1, pp. 46–55, 1999.
[2] F. Cayre and B. Macq, "Data hiding on 3-d triangle meshes," *Signal Processing, IEEE Transactions on*, vol. 51, no. 4, pp. 939–949, 2003.

[3] R. Ohbuchi, H. Masuda, and M. Aono, "Watermaking three-dimensional polygonal models," in *Proceedings of the fifth ACM international conference on Multimedia*. Seattle, Washington, United States: ACM, 1997, pp. 261–272.

[4] F. Bartolini, M. Barni, V. Cappellini, and A. Piva, "Mask building for perceptually hiding high frequency embedded watermarks," in *Image Processing, 1998. ICIP 98. Proceedings. 1998 International Conference on*, vol. 1, Oct 1998, pp. 450–454.

[5] M. Barni, F. Bartolini, and A. Piva, "Improved wavelet-based watermarking through pixel-wise masking," *Image Processing, IEEE Transactions on*, vol. 10, no. 5, pp. 783–791, May 2001.

[6] I. J. Cox and M. L. Miller, "Review of watermarking and the importance of perceptual modeling," B. E. Rogowitz and T. N. Pappas, Eds., vol. 3016, no. 1. SPIE, 1997, pp. 92–99.

[7] R. B. Wolfgang, C. I. Podilchuk, and E. J. Delp, "Perceptual watermarks for digital images and video," in *Society of Photo-Optical Instrumentation Engineers (SPIE) Conference Series*, vol. 3657, Apr. 1999, pp. 40–51.

[8] C. Podilchuk and W. Zeng, "Perceptual watermarking of still images," in *Multimedia Signal Processing, 1997., IEEE First Workshop on*, Jun 1997, pp. 363–368.

[9] C. Podilchu and W. Zeng, "Image-adaptive watermarking using visual models," *Selected Areas in Communications, IEEE Journal on*, vol. 16, pp. 525–539, May 1998.

[10] M. Corsini, E. D. Gelasca, T. Ebrahimi, and M. Barni, "Watermarked 3-d mesh quality assessment," *Multimedia, IEEE Transactions on*, vol. 9, no. 2, pp. 247–256, 2007.

[11] F. Uccheddu, M. Corsini, M. Barni, and V. Cappellini, "A roughness-based algorithm for perceptual watermarking of 3d meshes," in *Proceedings of the 10th internaltional conference on Virtual System and Multimedia*. ACM, 2004, pp. 934–943.

[12] J. A. Ferwerda, P. Shirley, S. N. Pattanaik, and D. P. Greenberg, "A model of visual masking for computer graphics," in *SIGGRAPH '97: Proceedings of the 24th annual conference on Computer graphics and interactive techniques*, New York, NY, USA, 1997, pp. 143–152.

[13] S. Kanai, H. Date, and T. Kishinami, "Digital watermarking for 3d polygons using multiresolution wavelet decomposition," in *IFIP WG*, 1998, pp. 296–307.

[14] A. Bors, "Watermarking mesh-based representations of 3-d objects using local moments," *Image Processing, IEEE Transactions on*, vol. 15, no. 3, pp. 687–701, 2006.

[15] F. Uccheddu, M. Corsini, and M. Barni, "Wavelet-based blind watermarking of 3d models," in *MM&Sec '04: Proceedings of the 2004 workshop on Multimedia and security*. ACM, 2004, pp. 143–154.

[16] M. Lounsbery, T. D. DeRose, and J. Warren, "Multiresolution analysis for surfaces of arbitrary topological type," *ACM Trans. Graph.*, vol. 16, no. 1, pp. 34–73, 1997.

[17] K. Kim, M. Barni, and H. Z. Tan, "Roughness-adaptive 3d watermarking of polygonal meshes," *Information Hiding: 11th International Workshop, Darmstadt, Germany, June 8-10, 2009*, pp. 191–205, 2009.

[18] J. Nelder and R. Mead, "A simplex method for function minimization," *The Computer Journal*, vol. 7, no. 4, pp. 308–313, 1965.

[19] H. Levitt, "Transformed up-down methods in psychoacoustics," *The Jounal of the Acoustical Society of America*, vol. 49, no. 2B, pp. 467–477, 1971.

[20] H. Gouraud, "Continuous shading of curved surfaces," *IEEE Trans. Comput.*, vol. 20, no. 6, pp. 623–629, 1971.

[21] O. Benedens and C. Busch, "Towards blind detection of robust watermarks in polygonal models," in *Computer Graphics Forum*, vol. 19 Issue 3, 2001, pp. 199–208.

[22] A. G. Bors, "Blind watermarking of 3d shapes using localized constraints," in *Proceedings of the 3D Data Processing, Visualization, and Transmission, 2nd International Symposium*. IEEE Computer Society, 2004, pp. 242–249.

[23] F. Cayre, P. Rondao-Alface, F. Schmitt, B. Macq, and H. Ma?re, "Application of spectral decomposition to compression and watermarking of 3d triangle mesh geometry," *Signal Processing: Image Communication*, vol. 18, no. 4, pp. 309–319, 2003, tY - JOUR.

[24] J. Cho, R. Prost, and H. Jung, "An Oblivious Watermarking for 3-D Polygonal Meshes Using Distribution of Vertex Norms," *IEEE Transactions on Signal Processing*, vol. 55, pp. 142–155, Jan. 2007.

[25] Z. Karni and C. Gotsman, "Spectral compression of mesh geometry," in *SIGGRAPH '00: Proceedings of the 27th annual conference on Computer graphics and interactive techniques*, 2000, pp. 279–286.

[26] J. Konstantinides, A. Mademlis, P. Daras, P. Mitkas, and M. Strintzis, "Blind robust 3-d mesh watermarking based on oblate spheroidal har-

monics," *Multimedia, IEEE Transactions on*, vol. 11, no. 1, pp. 23–38, Jan. 2009.

[27] H.-Y. Lin, H.-Y. Liao, C.-S. Lu, and J.-C. Lin, "Fragile watermarking for authenticating 3-d polygonal meshes," *Multimedia, IEEE Transactions on*, vol. 7, no. 6, pp. 997–1006, 2005.

[28] R. Ohbuchi, S. Takahashi, T. Miyazawa, and A. Mukaiyama, "Watermarking 3d polygonal meshes in the mesh spectral domain," in *GRIN'01: No description on Graphics interface 2001*, 2001, pp. 9–17.

[29] R. Ohbuchi and S. Takahashi, "A frequency-domain approach to watermarking 3d shapes," *Computer Graphics Forum*, vol. 21, no. 1, pp. 373–382, 2003.

[30] E. Praun, H. Hoppe, and A. Finkelstein, "Robust mesh watermarking," in *SIGGRAPH '99: Proceedings of the 26th annual conference on Computer graphics and interactive techniques*, New York, NY, USA, 1999, pp. 49–56.

[31] M. G. Wagner, "Robust watermarking of polygonal meshes," in *Geometric Modeling of Processing*, vol. 0, 2000, p. 201.

[32] K. Wang, G. Lavoue, F. Denis, and A. Baskurt, "Hierarchical watermarking of semiregular meshes based on wavelet transform," *Information Forensics and Security, IEEE Transactions on*, vol. 3, no. 4, pp. 620–634, Dec. 2008.

[33] J. Wu and L. Kobbelt, "Efficient spectral watermarking of large meshes with orthogonal basis functions," in *In The Visual Computers (Pacific Graphics 2005 Proceedings*, 2005, pp. 8–10.

[34] B.-L. Yeo and M. M. Yeung, "Watermarking 3d objects for verification," *IEEE Comput. Graph. Appl.*, vol. 19, no. 1, pp. 36–45, 1999.

[35] S. Zafeiriou, A. Tefas, and I. Pitas, "Blind robust watermarking schemes for copyright protection of 3d mesh objects," *Visualization and Computer Graphics, IEEE Transactions on*, vol. 11, no. 5, pp. 596–607, 2005.

Kwangtaek Kim received his Bachelor's and Master's degrees in Electronic Engineering from Korea University in 1998 and 2001, respectively. After graduation, he worked as a research engineer in the fields of biomedical imaging and digital image processing for several companies in Korea. Since August 2005, he has been a PhD student in the School of Electrical and Computer Engineering at Purdue University. His research interests include haptics-aware digital watermarking and haptics rendering. He is a student member of the IEEE.

Mauro Barni graduated in electronic engineering at the University of Florence in 1991. He received the PhD in informatics and telecommunications in October 1995. He has carried out his research activity for over 18 years first at the Department of Electronics and Telecommunication of the University of Florence, then at the Department of Information Engineering of the University of Siena where he works as associate Professor. During the last decade he has been studying the application of image processing techniques to copyright protection and authentication of multimedia (digital watermarking). He is author/co-author of about 200 papers published in international journals and conference proceedings, and holds three patents in the field of digital watermarking. He is co-author of the book "Watermarking Systems Engineering: Enabling Digital Assets Security and other Applications", published by Dekker Inc. in February 2004. He participated to several National and European research projects on diverse topics, including computer vision, multimedia signal processing, remote sensing, digital watermarking, IPR protection. In particular he is the coordinator of the project SPEED - Signal Processing in the EncryptEd Domain funded by the EC under the FP6 (FET - program). He is the editor in chief of the EURASIP Journal on Information Security. He serves as associate editor of the IEEE Trans. on Circuits and system for Video Technology and the IET Proceedings on Information Security. He was the general chairman of the 2004 edition of IEEE workshop on Multimedia Signal Processing (MMSP'04) and the 2005 edition of the International Workshop on Digital Watermarking (IWDW'05). He is the chairman of the IEEE Information Forensic and Security technical Committee (IFS-TC) of the IEEE Signal Processing Society. He is a senior member of the IEEE and EURASIP.

Hong Z. Tan received her Bachelor's degree in Biomedical Engineering (in 1986) from Shanghai Jiao Tong University and earned her Master and Doctorate degrees (in 1988 and 1996, respectively), both in Electrical Engineering and Computer Science, from the Massachusetts Institute of Technology (MIT). She was a Research Scientist at the MIT Media Lab from 1996 to 1998 before joining the faculty at Purdue University. She is currently an associate professor of electrical and computer engineering, with courtesy appointments in the school of mechanical engineering and the department of psychological sciences. She is an associate editor of Presence, ACM Transactions on Applied Perception and IEEE Transactions on Haptics. Tan was a co-organizer (with Blake Hannaford) of the International Symposium on Haptic Interfaces for Virtual Environment and Teleoperator Systems from 2003 to 2005. She served as the founding chair of the IEEE Technical Committee on Haptics, a home for the international interdisciplinary haptics research community, from 2006-2008. She was a recipient of the National Science Foundation CAREER award from 2000-2004, and a co-author of "Haptic feedback enhances force skill learning" that won the best paper award at the 2007 World Haptics Conference. Tan has published more than 110 peer-reviewed articles in journals and conference proceedings and 2 book chapters. Her research focuses on haptic human-machine interfaces in the areas of haptic perception, rendering and multimodal performance. She is a senior member of the IEEE and a member of the Psychonomic Society.